ADVANCED MATERIALS TECHNOLOGIES
www.advmattechnol.de

Construction of 3D Patterns Through Modified Electrochemical Replication and Transfer

*Zijian Chen, Jingjing Fu, Fan Chen, Chuan Xie, Qiuna Zhuang, Qiyao Huang, and Zijian Zheng**

As the development of flexible electronics continuously progresses, so does the demand for fabricated 3D electrodes via patterning technology. Electrochemical replication and transfer (ERT) has emerged as an efficient patterning technique, which deposits materials of interest on a predefined template via electroplating and subsequently transfers them onto target substrates. ERT can pattern large-area 2D electrodes on nontraditional substrates whilst maintaining adequate flexibility, stretchability, and complex surface structures. This study extends the capability of ERT from 2D into 3D patterning. Via the rational design of a 3D SiO_2/Si template, in which conductive Si trenches or holes are patterned with insulating SiO_2 banks, electroplating of materials only occurs in the exposed Si surfaces so that both continuous and isolated 3D patterns with high aspect ratios up to 4:1 are realized. 3D-ERT offers a high-throughput and low-cost approach to fabricating high Figure of Merit (>30 000) flexible transparent electrodes. Also, the application of 3D-ERT in constructing highly sensitive, and self-powered pressure sensors is showcased.

1. Introduction

In numerous emerging applications including metasurfaces,[1] sensors,[2–4] tissue engineering,[5] and energy harvesting and storage,[6–8] the fabrication of 3D patterns with high aspect ratios at the nano and micro-scale is critical due to the insightful improvements in physicochemical characteristics provided by such structures.[9,10] Meanwhile, the growing demand for the Internet of Things (IoT) has promoted the development of wearable electronic devices, most notably regarding the construction of 3D patterns equipped on unconventional substrates with sustained flexibility and stretchability.[11] The integration of these applications into the wearable system is as crucial as preserving its original, intrinsic performance.[12,13] Conventional lithography techniques like photolithography provoke considerable challenges facing the direct patterning process on flexible substrates. Advanced patterning techniques such as transfer printing,[14–17] inject printing,[18,19] 3D printing,[20–22] and soft lithography[23–26] have been proven as suitable substitutes that bypass the problems in flexible electronic fabrication like rough surfaces with low wettability, poor resistance to chemical solvents, or unstable in thermal treatment.[27] Nonetheless, achieving high-resolution and high-aspect ratio patterns on these substrates, whilst maintaining commercial requirements regarding throughput and cost, via existing pattern technologies remains an untouchable challenge.[28–31]

To address this challenge, a bottom-up patterning technology named electrochemical replication and transfer (ERT) was developed. ERT enables the repeatable and parallel fabrication of multi-scale patterns with resolutions spanning from sub-100 nm to multiple centimeters on flexible and stretchable substrates.[32] In this method, a gold (Au) patterned template was fabricated by conventional lithography techniques. It was used as the template for the electrodeposition of target materials on the patterned area due to the difference in conductivity between the Au pattern and silicon(Si) substrate. First, a self-assembled monolayer (SAM) of 1H,1H,2H,2H-perfluorodecanethiol (PFDT) was constructed on the Au template through the thiol groups at the chain terminal to reduce the adhesive force between the Au template and the target materials. As a result, the target patterns could easily be peeled

Z. Chen, F. Chen, Q. Zhuang, Q. Huang, Z. Zheng
School of Fashion and Textiles
The Hong Kong Polytechnic University
Hung Hom, Hong Kong SAR 999077, China
E-mail: tczzheng@polyu.edu.hk
J. Fu, C. Xie, Z. Zheng
Department of Applied Biology and Chemical Technology
The Hong Kong Polytechnic University
Hung Hom, Hong Kong SAR 999077, China
Q. Huang, Z. Zheng
Research Institute for Intelligent Wearable Systems
The Hong Kong Polytechnic University
Hung Hom, Hong Kong SAR 999077, China
Z. Zheng
State Key Laboratory for Ultra-precision Machining Technology
The Hong Kong Polytechnic University
Hung Hom, Hong Kong SAR 999077, China
Z. Zheng
Research Institute for Smart Energy
The Hong Kong Polytechnic University
Hung Hom, Hong Kong SAR 999077, China
The ORCID identification number(s) for the author(s) of this article can be found under https://doi.org/10.1002/admt.202301695

DOI: 10.1002/admt.202301695

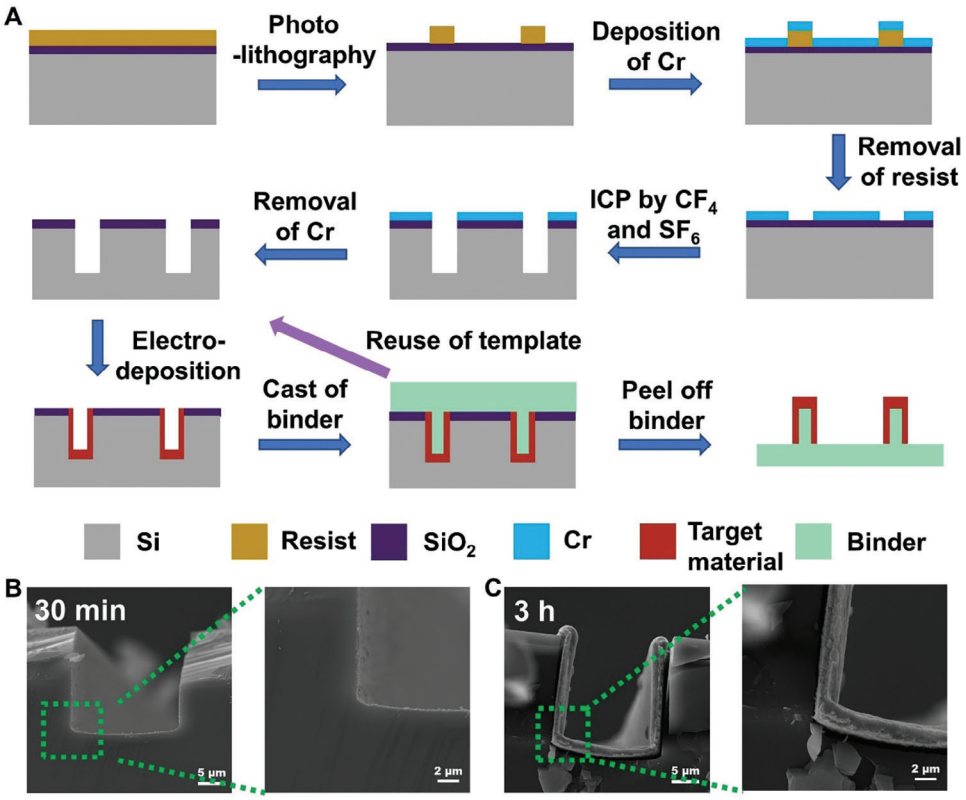

Figure 1. The 3D-ERT for the fabrication of 3D structure patterns. A) Schematic illustration of the template fabrication process and transfer of the electrodeposited pattern. B) The cross-section SEM images of a 3D-ERT template after 30 min of electroplating of Cu. C) The same template after 3 h of electroplating of Cu. Current density: 1 mA cm^{-2}.

off and transferred to arbitrary flexible substrates using a binder layer without applying damage to the template, hence proving the balance ERT achieves regarding resolution (sub-100 nm), throughput (>10^2 m^2 h^{-1}), and cost (<$10 k). Furthermore, the obtained 2D electrodes show smooth surfaces with replicated patterns embedded in the binder layer, which improves the flexibility of the devices. However, the construction of 3D electrodes with ERT to satisfy the needs of further applications is yet to be demonstrated.

In this study, we extend the capability of ERT from 2D to 3D by using a 3D SiO_2/Si template for the fabrication of flexible 3D electrodes. Through simple photolithography and an inductively coupled plasma (ICP) etching process, the 3D Si template with a SiO_2-protected surface can be fabricated without Au deposition. It can fabricate both continuous and isolated patterns with different conductive materials due to the selective growth of such materials on the exposed Si surface during electrodeposition to replicate the 3D template's structure. The hard properties of Si also ensure the reusability of the template. Moreover, the growth of target materials is confined to the 3D grooves area, thus preventing the decrease in resolution which would otherwise be caused by isotropic growth of materials during electrodeposition using the conventional 2D template. Therefore, 3D-ERT is suitable for the fabrication of high-aspect-ratio mesh patterns applied for flexible transparent electrodes due to its ability to achieve low sheet resistance (R_s) without compromising transparency (T). By adjusting the line width and gaps of the mesh pattern, we obtain an ultrahigh Figure of Merit (FoM) value exceeding 30 000. The flexible transparent electrode can be applied to flexible transparent heaters with a short response time and high power efficiency. Additionally, the 3D-ERT method can also be applied for fabricating complex multilayer 3D microstructures for pressure sensors, which are proven to be beneficial for enhancing sensitivity.

2. Results and Discussion

2.1. Fabrication and Transfer Process of 3D-ERT

Figure 1 illustrates the entire fabrication and transfer process of 3D structure patterns through 3D-ERT. Photolithography, as one of the conventional lithography methods to generate patterns, is first conducted on a Si wafer with a specific thickness of SiO_2 (e.g., 500 nm), depending on the application. Following this, with chromium (Cr) as an etching mask in ICP dry etching, SiO_2, and Si are etched by CF_4 and SF_6 gas, respectively. The height of the replicated 3D pattern is determined via the etching depth of the Si layer. Regarding the reduced adhesive force between Si and the target materials, the SiO_2/Si template is immersed in a silylating reagent for 10 min and heated at 120 °C for 15 min, forming a hydrophobic molecular layer on the Si surface to ease the peeling-off process. The target materials only deposit onto the exposed surface of Si since SiO_2 is an insulator, inclusive of both the bottom and lateral areas of the patterned grooves. Finally, a UV-curable

binder NOA 63 is cast onto the surface and fills the entire groove. The target materials are peeled off effortlessly whilst the sustainable 3D template can be reused for future fabrication. The replication and transfer processes are the same as those of the original ERT process, thus permitting the preservation of ERT's advantages in high resolution, large-area fabrication, and efficient cost.[32]

As shown in Figure 1B,C, the scanning electron microscope (SEM) images characterize the growth of electrodeposited materials on the 3D template, illustrating the cross-sectional area of a 3D template with a width and depth of 20 μm. After 30 min of electroplating at a current density of 1 mA cm^{-2}, only a thin layer of copper (Cu) (≈100 nm) was deposited on the surface of the exposed Si area, including both the bottom and side walls of the groove. Following an extended deposition time (3 h), the thickness of the Cu layer increased to ≈2 μm. Despite the restriction that the insulating SiO_2 layer (≈500 nm) was implanted, Cu was able to grow out of the groove after a prolonged period of time. To utilize this limited growth, the SiO_2 layer needs to be increased under specific circumstances.

2.2. Fabrication of 3D Patterns

To demonstrate the efficacy of the 3D structure in maintaining high resolution, 3D line pattern templates with a depth of 20 μm were fabricated. The corresponding 3D Cu patterns were fabricated and transferred to polyethylene terephthalate (PET) substrates. Optical images in **Figure** 2A,B detail the template with 20 μm line width after electroplating as well as the Cu pattern following transfer with electroplating times of 30 min and 3 h, respectively. As observed, the Cu patterns left no damage when peeled off the template and the line widths (with varying line pattern resolutions including 5, 10, and 20 μm) remained practically unchanged despite electroplating for 3 h (Figure S1, Supporting Information), thus proving the success of the Cu pattern fabrication. Such success was confirmed by the energy dispersion X-ray (EDX) results of the Cu element during the complete fabrication process, including the initial 3D Si template, the 3D Si template after the electroplating process, and the Cu patterns on the PET substrate after the peeling-off process (Figure 2C–E).

The incessant study of etching of Si for high aspect ratio (AR) over past decades has facilitated the fabrication of 3D structure templates with various resolutions and depths.[33] For this 3D-ERT template, the highest resolution of the lines pattern reaches up to 2 μm (Figure S2, Supporting Information), with an AR of 1:1. As shown in the cross-section SEM images in Figure 2F, Cu lines patterns were successfully fabricated in 30 min through electroplating. Given that the Cu lines patterns had different line widths (5, 10, and 20 μm), the highest AR could reach 4:1 for the 5 μm lines pattern. Modification of the silylating reagent significantly reduced the surface energy of the Si substrate, formulating a substrate that is suitable for the peeling-off of various materials like Au, Ag, and Ni (Figure 2G).[34] Other than continuous line patterns, the 3D-ERT template can also be applicable for fabricating isolated patterns. Despite the concealing covering of the insulated SiO_2 layer, the electroplating process proceeded smoothly because the silicon substrate ensured the electric current transmission. Therefore, as demonstrated in Figure 2H–K and Figure S3 (Supporting Information), isolated Cu dots arrays (AR-1:2) with circles and squares were fabricated and transferred to PET substrates, leaving no damage (Figure 2H,I). The corresponding EDX result of Cu and the cross-section image of SEM are also presented (Figure 2J,K).

2.3. The 3D Metal Meshes for Flexible Transparent Electrodes

Metal mesh pattern electrodes have been deemed an excellent option for flexible transparent electrodes (FTEs) due to the remarkably perfect balance it has between R_s and T.[35,36] Moreover, the geometric features of the mesh pattern are capable of effortless adjustments which aid the improvement of its overall electro-optical performance.[37,38] Here, we approached the development of a 3D structure FTE by employing the 3D-ERT method for the fabrication of a Cu mesh electrode. This innovative method enables precise control over the resolution of the pattern, leading to a harmonious balance between R_s and T. As an example, we selected a mesh pattern with a 5 μm line width and a 200 μm gap based on previous research.[32] As seen in **Figure** 3A,B and Figures S4 and S5 (Supporting Information) the optical images depict the retained benefits of the 3D-ERT method during the fabrication process of the mesh pattern. Regarding the original 2D-ERT template, the line width faced greatly increases from 5 to ≈20 μm when undergoing electroplating from 5 min to 3 h under a current density of 1 mA cm^{-2}. On the other hand, the line width of the 3D Cu mesh pattern faced little changes despite 6 h of electroplating. The entire 3D structure remained completely intact during the transfer process as revealed from the optical surface profiler image of the 3D Cu mesh pattern on PET with an approximate height of 10 μm (Figure S6, Supporting Information).

Given that the transparency of the mesh pattern electrode is highly correlated to the line parameters (line width and line gap), it suggests that the performance of transparency is also significantly dependent on the following electroplating time in ERT. As the electroplating time of the 2D-ERT-fabricated Cu mesh electrodes increased from 5 min to 3 h, its original transmittance at 550 nm decreased from 91.03% to 82.37%. Whereas, the transmittance for the 3D Cu mesh pattern remained constant at ≈88% despite 6 h of electroplating (Figure 3C). Additionally, the R_s of both 2D and 3D Cu mesh patterns decreased rapidly after 1 h of electroplating. The trend began to level off after 3 h of electroplating (Figure 3D). To combat this challenge, we further adjusted the parameters of the mesh electrodes, hence achieving a better R_s-T balance. To experiment, we electroplated various Cu mesh electrodes for 3 h with different line widths, gaps, and heights. Optical images and transmittance results (Figures S7 and S8, Supporting Information; Figure 3E, respectively) demonstrated a relatively low sheet resistance for all the samples. The sheet resistance and transmittance both attain an extensive adjustable range. All detailed data of the Cu mesh electrodes fabricated in this experiment, including parameters, transmittance, and sheet resistance, were listed in **Table** 1. The Figure of Merit (FoM) value, which is typically used to evaluate FTEs' performance,

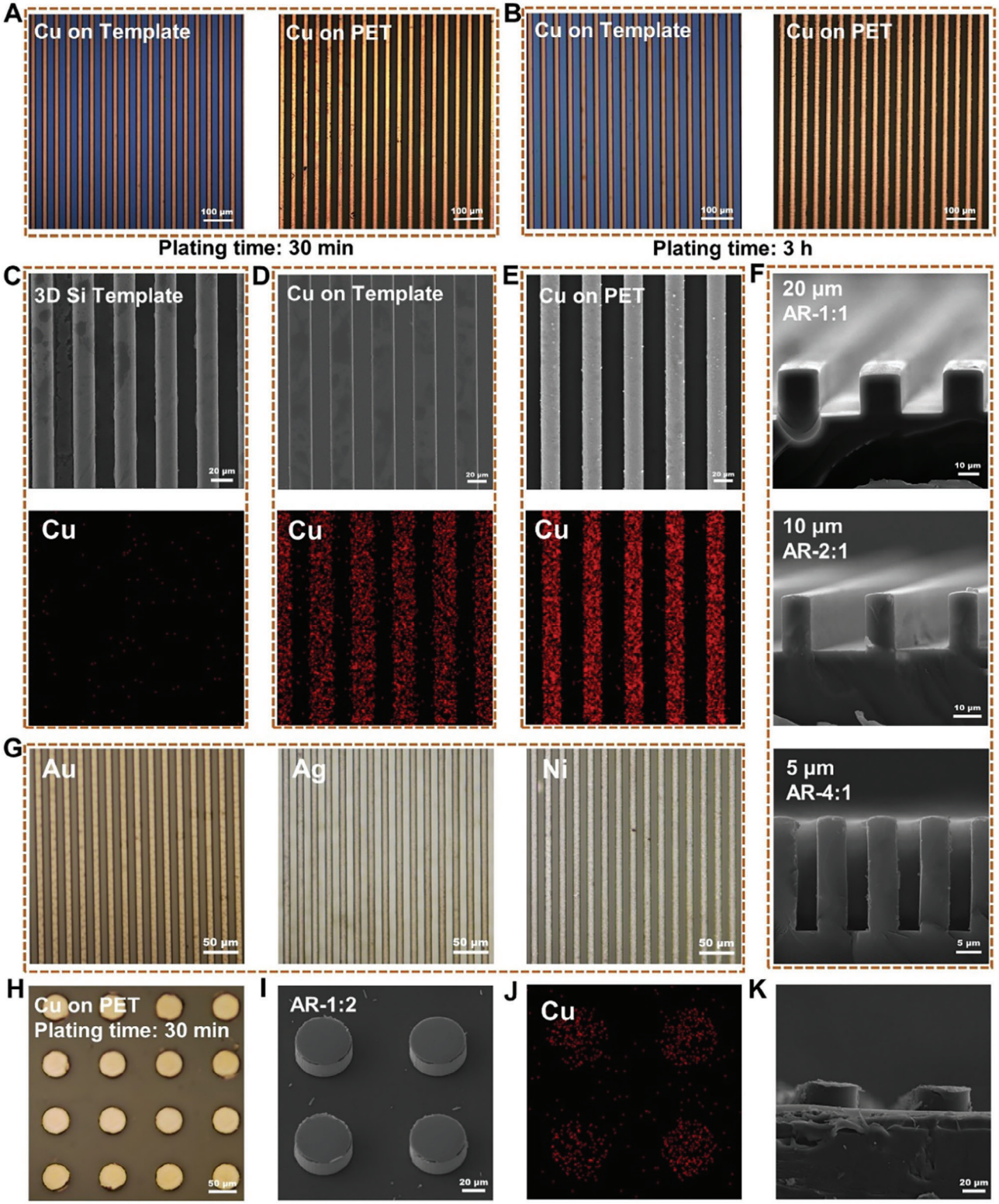

Figure 2. Fabrication of various patterns with different resolutions, aspect ratios, materials, and shapes. A) Optical images of 3D pattern template with 20 μm lines pattern after 30 min of Cu deposition and peeled off by PET substrate. B) Optical images of 3D pattern template after 3 h of Cu deposition and peeled off by PET substrate. C) SEM image and EDX result of Cu of the 3D Si template. D) SEM image and EDX result of Cu of the 3D template after Cu deposition. E) SEM image and EDX result of Cu of the lines pattern peeled off by PET. F) Cross-section SEM image of 20 μm lines, 10 μm lines, and 5 μm lines with 20 μm height. G) Optical images of 10 μm 3D lines with different materials including Au, Ag, and Ni. H) Optical image of 50 μm 3D dots array pattern peeled off by PET. I) SEM image of the 3D dots array with a 1:2 aspect ratio. J) EDX result of the Cu. K) Cross-section SEM image.

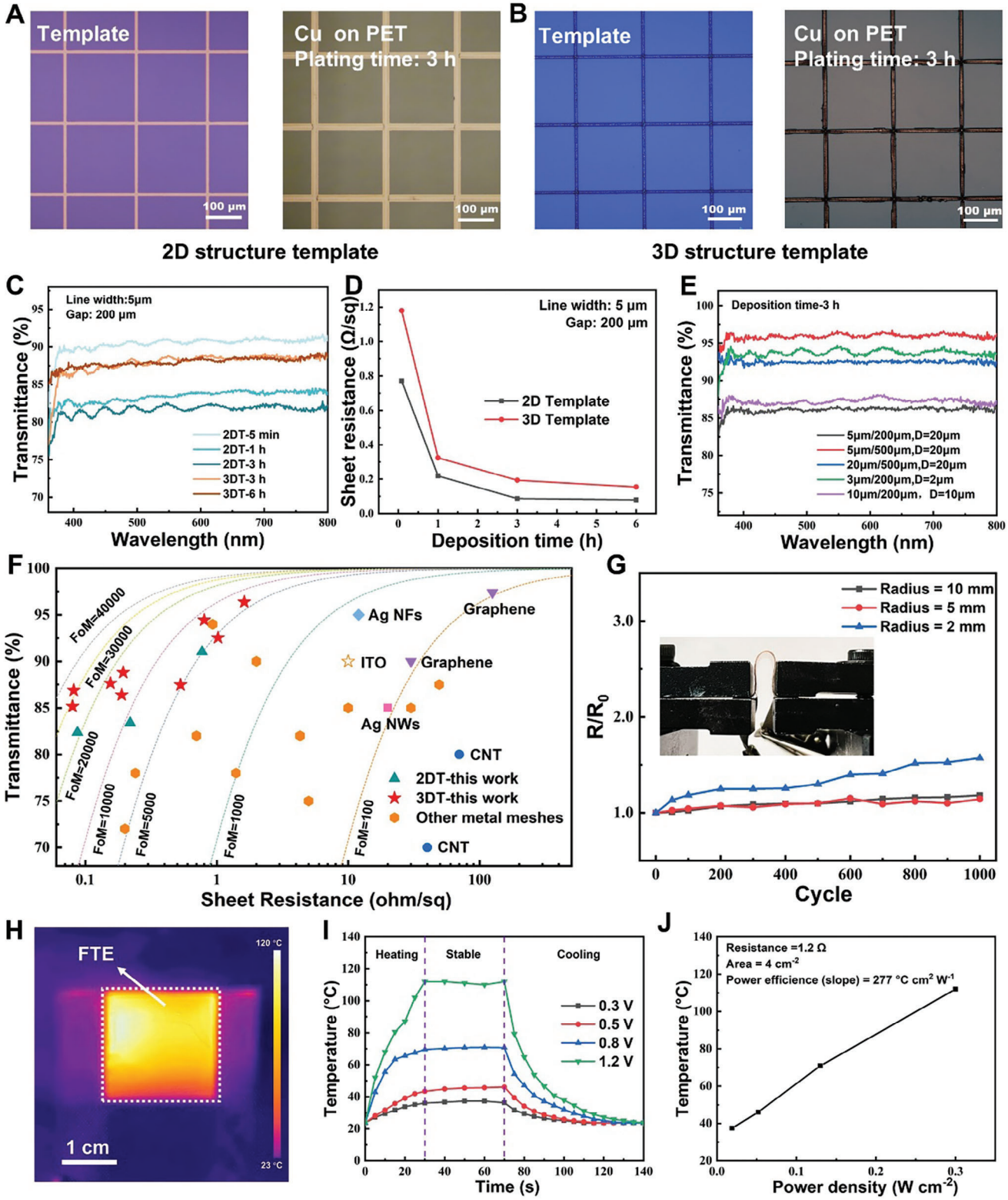

Figure 3. Application of 3D mesh pattern for flexible transparent electrodes. A) Optical images of the mesh pattern template fabricated by the original ERT method and the Cu mesh pattern peeled off by PET after 3 h of electrodeposition. B) Optical images of the mesh pattern template fabricated by the 3D structure ERT method and the Cu mesh pattern peeled off by PET after 3 h of electrodeposition. C) UV–vis spectra of the mesh pattern electrodes fabricated by the original and 3D template with different electroplating times. D) Sheet resistance versus electroplating time of the mesh pattern electrodes fabricated by the original and 3D template. E) UV–vis spectra of the mesh pattern electrodes fabricated by the 3D structure template

Table 1. Parameters and performance of all the 3D FTEs.

	Grid (μm/μm)	Height (μm)	Transmittance at 550 nm (%)	Sheet resistance (Ω sq^{-1})	FoM
2DT-5 min	5/200	0	91.03	0.7715	5078
2DT-1 h			83.39	0.2190	9053
2DT-3 h			82.37	0.0870	21 276
3DT-30 min	10/200	10	87.48	0.5301	5141
3DT-3 h			86.89	0.0815	31 774
3DT-6 h			85.16	0.0799	28 209
3DT-3 h	5/200	10	88.81	0.1940	15 895
3DT-6 h			87.64	0.1550	17 834
3DT-3 h	5/200	20	86.40	0.1889	13 160
3DT-3 h	5/500	20	96.39	1.6187	6276
3DT-3 h	20/500	20	92.54	1.0210	4670
3DT-3 h	3/200	2	94.43	0.8012	8093

was also calculated based on Equation (1) below and listed in the table[39]:

$$FoM = \frac{188.5}{R_s\left(\frac{1}{\sqrt{T}} - 1\right)} \quad (1)$$

Among all the transparent electrodes mentioned in this paper, the transparent mesh pattern electrode with a 10 μm line width, 200 μm line gap, and 10 μm height, exhibits the best overall performance. It achieves a transmittance of 86.89% at 550 nm, a sheet resistance of 0.0815 Ω sq^{-1}, and an exceptional FoM of 31 774. Compared with previously reported FTEs, including Indium Tin Oxide (ITO),[40] Ag nanowires,[41] carbon nanotubes,[42] graphene,[43] Ag nanofibers,[44] and other metal meshes,[45–51] the performance of our 3D Cu mesh pattern FTE significantly surpasses over others as reiterated from the above statistics (Figure 3F). The fabrication of a large-scale (four-inch) electrode could also be realized (Figure S9, Supporting Information).

As the 3D mesh pattern is raised on the surface of the PET substrate, the encapsulation process is vital in ensuring the electrode's flexibility. Additional NOA 63 was chosen as the encapsulation material (Figure S10, Supporting Information). This extra layer of NOA 63 binder serves as protection to prevent cracking of the metal during the bending process, as demonstrated from the testing status of the encapsulated electrodes at a minute bending radius of 2 mm (Figure 3G). Despite being bent at a radius of 2 mm for 1000 cycles, the ratio of the change in resistance is yet lower than a mere 1.5.

The infrared radiation (IR) image taken at a constant input voltage of 1.2 V proves that the encapsulated 3D FTEs could be applied as electrodes for flexible transparent heaters (FTHs) (Figure 3H). It is capable of reaching up to 114 °C with a homogeneous distribution of heat. Moreover, Figure 3I indicates that the heater's temperature can be freely adjusted from 30 to 114 °C as voltage ranges from 0.3 to 1.2 V. The heating process finishes within 30 s and then remains stable at its maximum temperature. The output power density can be calculated based on the maximum temperature at different input voltages, as shown in Figure 3J. The slope of the plot reflects the high-power efficiency of our FTH reaching 277 °C cm^2 W^{-1}.

2.4. The 3D Structures for Flexible Pressure Sensors

The sensor is an indispensable part of a wearable integrated system to monitor and reflect the response of the human body.[52,53] The performance of sensors largely depends on the sensitivity to various stimulations.[54,55] An effective method to enhance the compressibility and sensitivity of sensors is through constructing microstructures on the electrodes.[56,57] However, the manufacturing of various microstructures, such as pyramids, hemispheres, pillars, and porosity, often requires sophisticated, expensive, and complex methods that are not appropriate for large-scale preparations (e.g., photolithography on Si molds).[58,59] Therefore, the considerable advantages in large-scale replication models that the 3D-ERT method is equipped with make it a suitable technique for fabricating flexible pressure sensors with complex microstructures. As a proof of concept, we fabricated a triboelectric nanogenerator (TENG) based flexible pressure sensor using the 3D-ERT fabricated Cu electrode. As shown in **Figure 4**A, the TENG-based pressure sensor consists of a Cu-polydimethylsiloxane(PDMS)-Cu sandwich construction. The top Cu layer serves as an electrode, while the bottom Cu layer functions as both an electrode and a friction material that contacts PDMS. As the pressure increases, the contact area between the Cu and the PDMS gradually increases as well, leading to more triboelectric charges. On the other hand, the space between the two electrodes is compressed, causing the equivalent capacitance of the device to increase. The synergistic combination of these two effects results in the sensor's high sensitivity to pressure changes.

To further investigate the mechanism of the TENG-based sensor, we fabricated array pattern electrodes with circle dots (d = 50 μm, *d*: diameter) at varying heights (4, 14, and 20 μm) (Figure 4B,C; Figure S11, Supporting Information). As illustrated in Figure 4D, the relationship between the normalized voltage of the tested sensors and the applied pressure is positive throughout. During the low-pressure range (0–5 kPa), it can be observed that the pressure sensitivity is insignificantly dependent on the height as it remains at ≈0.6 kPa^{-1} for all samples. However, taller heights imply a larger detection range that induces a higher output. In the high-pressure range (>5 kPa), the sensitivity decreased and the impact of circle heights was further reduced.

with different line widths, gaps, and heights. F) Comparison of optoelectronic performance between our 3D Cu mesh-based FTEs and other typical TEs published previously, including Indium Tin Oxide (ITO),[40] Ag nanowires,[41] carbon nanotubes,[42] graphene,[43] Ag nanofibres,[44] other metal meshes.[45–51] G) The resistance change of the mesh pattern electrodes with 10 μm width, 200 μm gap, and 10 μm height at different bending radii. Insert image: Digital image of the sample during the bending test. H) Demonstration of a flexible transparent heater (FTH) based on 3D mesh pattern electrodes. IR image of the transparent electrode at a constant input voltage (1.2 V). I) The temperature profile of the FTH as a function of the time while applied with different voltages. J) The plot of the FTH temperature at steady state versus calculated input power density.

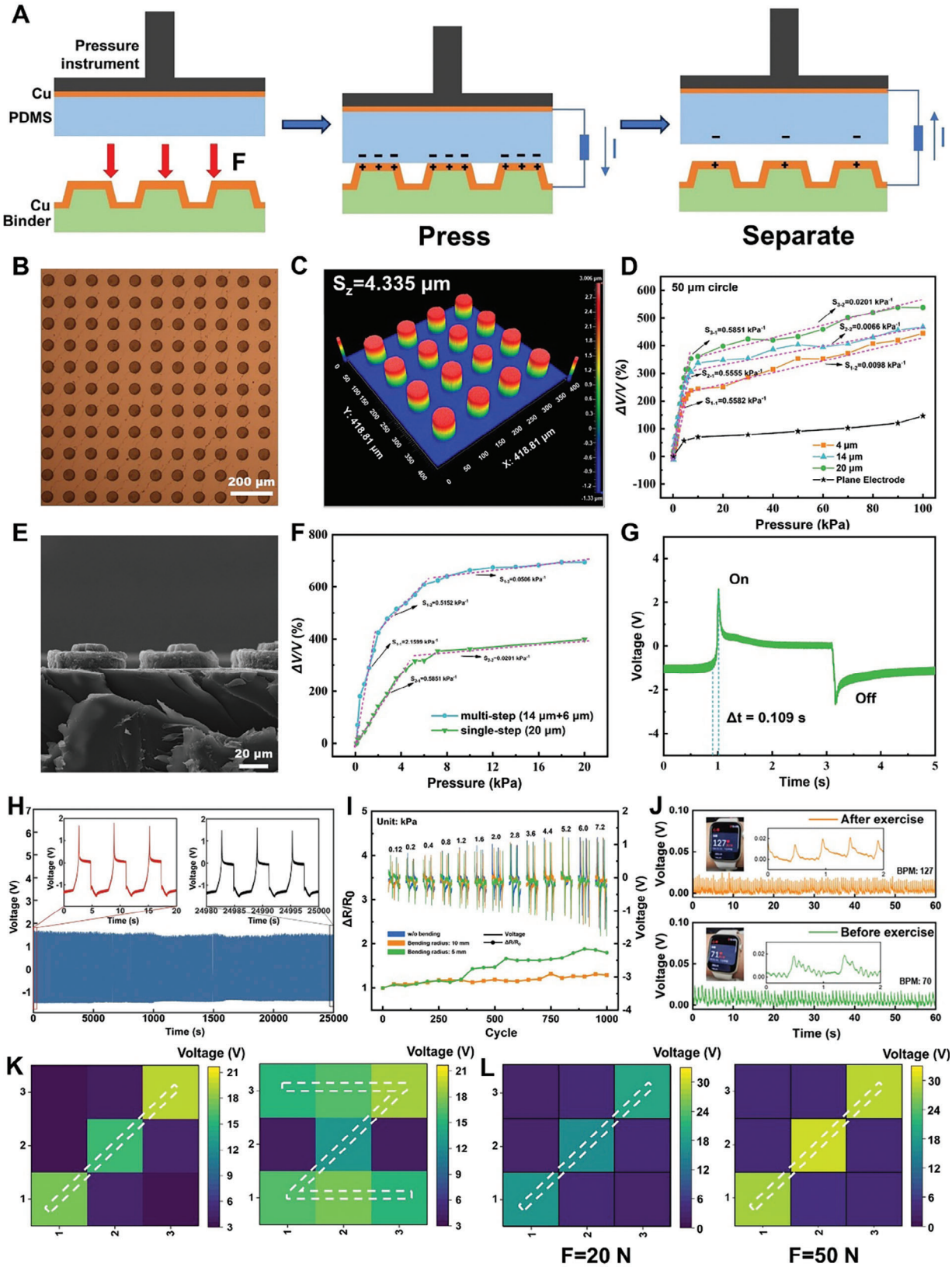

Figure 4. Fabrication of 3D dots array pattern for self-powered pressure sensors. A) Illustration of the structure of 3D dots array-based electrodes for the self-powered pressure sensor and the working mechanism. B) Optical image of the 3D Cu dots array electrode for the pressure sensor. C) Optical profiler image of the dots array. D) The pressure sensitivity of the sensors with different array heights. E) Cross-section SEM images of the multi-step

To further manipulate the advantages of 3D-ERT in constructing complex 3D structures, a multi-step 3D dots array pattern was fabricated. Its lower layer consists of the circle dots with a diameter of 50 μm and a height of ≈10 μm, and the upper layer consists of the concentrically fitted circle dots with a diameter of 20 μm and a height of ≈4 μm (Figure 4E). Compared to the single-step electrode sensor with the same height (the green line), the multi-step electrode sensor (the blue line) has a significantly higher sensitivity of 2.2 kPa^{-1} in the low-pressure range (0–2 kPa) (Figure 4F). It is also capable of a rapid response rate, reaching only 0.109 s (Figure 4G). The TENG-based sensor fabricated by 3D-ERT has prominent stability as the voltage output signal degradation was negligible after 25 000 s at a vertical pressure of 5 kPa (Figure 4H). It also exhibits impressive bending stability due to the flexibility of the substrate (Figure 4I). When the sensors composed of circle dots (d = 50 μm) array pattern electrodes were bent at different radii (10 and 5 mm) for 1000 cycles, the voltage signals maintained good stability at the whole testing range. The resistance of the devices also only showed a slight increase after the bending process.

Owing to the high sensitivity and stability characteristics of the flexible pressure sensor, it succeeds in being a reliable monitor to measure the pulse of the carotid artery. In this study, the sensor was attached to a human neck via medical tape and investigated for voltage signals before and after 5 min of exercise. The results show that the pre-exercise beat per minute (BPM) is ≈70 while the postexercise BPM is ≈127, which is consistent with the commercial watches (Figure 4J). Utilizing the fast replication and dimensional precision of 3D-ERT, a 3 × 3 sensor array could be easily fabricated in a cm-level device as shown in Figure S11 (Supporting Information). The voltage signal could both reveal the trace of finger writing (Figure 4K) and reflect different pressures (20 and 50 N) with the same mold in Figure S12 (Supporting Information) (Figure 4L).

3. Conclusion

To explore the field of flexible 3D electrodes and improve the construction of 3D patterns, we developed a novel 3D SiO_2/Si template through lithography and ICP etching for ERT. The templates not only are equipped with easily manufactured patterns and aspect ratios, but the different electrical conductivities of Si and SiO_2 endow selective electrodeposition of materials on the exposed surface of Si. The adoption of a 3D template in ERT allows for the facile fabrication and transfer of various patterns, not limited to continuous lines and isolated dots of different materials. It also eliminates the decreasing of resolution which would be caused by the isotropic growth of the electrodeposited materials. Importantly, 3D-ERT is advantageous in achieving not only a balance between resolution and throughput but also minimizing costs. Furthermore, this modified 3D-ERT method is also greatly advantageous in the fabrication of FTEs in the field of extending plating time without interfering with resolution. By adjusting the parameters of the FTEs, a high FoM value exceeding 30 000 was obtained. Finally, 3D-ERT is also suitable for applications that require the construction of complex 3D structures, such as pressure sensors. We envisage that 3D-ERT will become an indispensable component of the ERT method that will contribute to flexible electronic and photonic devices in the near future.

4. Experimental Section

Materials: Gold (Au, 99.999%, China New Metal),cchromium (Cr, 99.9%, China New Metal, China), doped silicon wafer with silicon oxide layer (SiO_2, 500 nm, Suzhou Crystal Silicon Electronic & Technology CO., Ltd, China), positive photoresist (AZ 5214E, Microchemicals GmbH, Germany), developer for AZ 5214E (AZ 300 MIF, Microchemicals GmbH, Germany), negative photoresist (NR9-1500P, Futurrex, Inc., USA), developer for NR9-1500P (DR6, Futurrex, Inc., USA), positive photoresist (AZ MiR 701, MicroChemicals, GmbH), developer for AZ MiR 701 (AZ 726 MIF, MicroChemicals, GmbH), Au etchant (Transene Company, Inc.), Cr etchant (Sigma-Aldrich), methyl isobutyl ketone (99.5%, Sigma-Aldrich), acetone (99.9%, Sigma-Aldrich), ethanol (99.5%, Sigma-Aldrich), isopropanol (99.5%, Sigma-Aldrich), 1H,1H,2H,2H-Perfluorodecanethiol (PFDT, 97%, Sigma-Aldrich), dodecyl triethoxysilane (UP-151, Nanjing UP Chemical Co. Ltd., China), commercial copper / gold / nickel / zinc plating solutions (Plug N Plate Cu Solution, Plug N Plate Au Solution, Plug N Plate Ni Solution, Plug N Plate Zn Solution, Caswell Inc., USA), Norland Optical Adhesive 63 (NOA 63, Norland Products Inc., USA), polyethylene terephthalate (PET, Suzhou Dawan Plastic Electronics Co. Ltd., China), Polydimethylsiloxane (PDMS, SYLGARD 184 Silicone Elastomer Kit, Germany).

Fabrication of 3D-ERT Si Substrate: The bare SiO_2/Si substrate was spin-coated with negative photoresist NR9-1500P at 4000 rpm for 40 s and prebaked on a hotplate at 155 °C for 1 min. The photoresist was then covered with the as-designed photomask and exposed to UV light with a dose of 170 mJ cm^{-2} on the mask aligner MA6. Subsequently, it was baked at 105 °C for 3 min, developed in DR6 developer for 10–15 s, rinsed in DI water, and dried with compressed N_2. Thermal evaporation deposited the photoresist-patterned substrate with a 50-nm-thick Cr layer. The photoresist and redundant deposited metals were washed away using acetone and ethanol. The resulting Cr pattern served as the mask for the following dry etching process. The SiO_2 and Si layers were etched in sequence using inductively coupled plasma reactive ion etching (ICP-RIE, Trion Phantom III, USA). For SiO_2, CF_4 gas was used at a flow rate of 40 sccm, ICP power was set to 1500 W, and RIE power was set to 32 W. The etching time was 500 s. For Si, SF_6 gas was used at a flow rate of 50 sccm, RIE power was set to 200 W, and the etching speed was ≈1 μm min^{-1}. After the dry etching process, the Cr mask residue was removed by immersing the template in the Cr etching solution for 10 min at 80 °C. Finally, the 3D-ERT template was obtained after washing with DI water and drying with compressed N_2.

3D-ERT Process: The as-fabricated 3D-ERT template was first immersed in a 20% dodecyl triethoxysilane ethanol solution for 10–12 min to form a molecular surface on the exposed Si surface. The Si template was then heated at 120 °C for 15 min and washed with ethanol. Subsequently, the template was ready for the following electroplating process. The electrodeposition process could be carried out by the two-electrode

dots array pattern electrode. F) Comparison of the pressure sensitivity of the multi-step sensor and the one-step sensor with the same circle dot height. G) Response time of multi-step array sensor at a pressure of 5 kPa. H) The voltage of the sensor with circle dots array of 50 μm diameter and 20 μm height over 25 000 s of compression-release cycles at a vertical pressure of 5 kPa. I) The resistance change of the sensor with circle dots array of 50 μm diameter and 20 μm height at different bending radii after 1000 cycles and the corresponding voltage signal at different pressures after the bending test. J) Application for pulse monitoring at resting and exercise state. Insert digital images: Commercial smartwatches showing heart rates. (K) A 3 × 3 sensor array shows the trace of writing by a human finger. L) A 3 × 3 sensor array shows the voltage output of a square-shaped mold under different pressures.

setup on a source meter (Keithley 2400, Tektronix, Inc., USA) or the three-electrode setup on an electrochemical workstation (CHI 600e, CH Instruments, Inc., China). The modified 3D-ERT template was used as the working electrode in the electrochemical deposition. The counter electrode was the dissolvable pure target material (such as Cu foil, Ni foil, or Zn foil) or a noble platinum (Pt) foil. In the three-electrode setup, an Ag/AgCl electrode served as the reference electrode. After the target material was deposited on the template, the template was rinsed with DI water and dried under compressed N_2. Then, NOA 63 was cast directly on the template and cured under 365 nm UV light with a dose of more than 4500 mJ cm^{-2}. The thickness of the cured adhesive polymer NOA 63 was ≈100 µm. To facilitate peeling off the target material pattern from the template, a transparent PET layer was covered on top of the uncured adhesive polymer NOA 63. After transferring the target material pattern, the Au-patterned template was rinsed with DI water and ethanol for reuse in subsequent fabrications.

Supporting Information

Supporting Information is available from the Wiley Online Library or from the author.

Acknowledgements

The authors acknowledge the financial support from the RGC Senior Research Fellowship Scheme (SRFS2122-5S04) and State Key Laboratory for Ultra-precision Machining Technology (1-BBXR). The authors thank Miss Chunyue Joey Zheng for her help in polishing the language.

Conflict of Interest

The authors declare no conflict of interest.

Author Contributions

Z.J.C. and Z.J.Z. performs conceptualization, data analysis, and wrote, reviewed, and edited. Z.J.C., J.J.F., C.X., Z.J.Z. Performs Idea discussion and Wrote—original draft. Z.J.C., J.J.F., F.C., Q.N.Z. Experimented. Z.J.Z., Q.Y.H. performs supervision.

Data Availability statement

The data that support the findings of this study are available in the supplementary material of this article.

Keywords

3D, additive manufacture, flexible electronics, pattern transfer

Received: October 6, 2023
Revised: January 3, 2024
Published online: January 17, 2024

[1] H.-H. Hsiao, C. H. Chu, D. P. Tsai, *Small Methods* **2017**, *1*, 1600064.
[2] S. Kasani, K. Curtin, N. Wu, *Nanophotonics* **2019**, *8*, 2065.
[3] Z. Liu, D. Qi, W. R. Leow, J. Yu, M. Xiloyannnis, L. Cappello, Y. Liu, B. Zhu, Y. Jiang, G. Chen, L. Masia, B. Liedberg, X. Chen, *Adv. Mater.* **2018**, *30*, 1707285.
[4] Q. Tang, H. Guo, P. Yan, C. Hu, *EcoMat* **2020**, *2*, e12060.
[5] W. Zhu, X. Ma, M. Gou, D. Mei, K. Zhang, S. Chen, *Curr. Opin. Biotechnol.* **2016**, *40*, 103.
[6] M. Muthu, R. Pandey, X. Wang, A. Chandrasekhar, I. A. Palani, V. Singh, *Nano Energy* **2020**, *78*, 105205.
[7] X. Zhou, P. S. Lee, *EcoMat* **2021**, *3*, e12098.
[8] W. He, C. Wang, H. Li, X. Deng, X. Xu, T. Zhai, *Adv. Energy Mater.* **2017**, *7*, 1700983.
[9] K. J. Mchugh, T. D. Nguyen, A. R. Linehan, D. Yang, A. M. Behrens, S. Rose, Z. L. Tochka, S. Y. Tzeng, J. J. Norman, A. C. Anselmo, X. Xu, S. Tomasic, M. A. Taylor, J. Lu, R. Guarecuco, R. Langer, A. Jaklenec, *Science* **2017**, *357*, 1138.
[10] M. M. Hossain, M. Gu, *Laser Photonics Rev.* **2014**, *8*, 233.
[11] T. G. Stavropoulos, A. Papastergiou, L. Mpaltadoros, S. Nikolopoulos, I. Kompatsiaris, *Sensors* **2020**, *20*, 2826.
[12] M. J. Cima, *Nat. Biotechnol.* **2014**, *32*, 642.
[13] J. S. Heo, J. Eom, Y.-H. Kim, S. K. Park, *Small* **2018**, *14*, 1703034.
[14] M. A. Meitl, Z.-T. Zhu, V. Kumar, K. J. Lee, X. Feng, Y. Y. Huang, I. Adesida, R. G. Nuzzo, J. A. Rogers, *Nat. Mater.* **2006**, *5*, 33.
[15] K. Sim, S. Chen, Z. Li, Z. Rao, J. Liu, Y. Lu, S. Jang, F. Ershad, J. Chen, J. Xiao, C. Yu, *Nat. Electron.* **2019**, *2*, 471.
[16] X. Chen, W. Jian, Z. Wang, J. Ai, Y. Kang, P. Sun, Z. Wang, Y. Ma, H. Wang, Y. Chen, X. Feng, *Sci. Adv.* **2023**, *9*, eadi0357.
[17] Q. Zhuang, K. Yao, M. Wu, Z. Lei, F. Chen, J. Li, Q. Mei, Y. Zhou, Q. Huang, X. Zhao, Y. Li, X. Yu, Z. Zheng, *Sci. Adv.* **2023**, *9*, eadg8602.
[18] W. Cheng, Y. Liu, Z. Tong, Y. Zhu, K. Cao, W. Chen, D. Zhao, H. Yu, *EcoMat* **2023**, *5*, e12288.
[19] Y. Shen, L. Yao, Z. Li, J. Kou, Y. Cui, J. Bian, C. Yuan, H. Ge, W.-D. Li, W. Wu, Y. Chen, *Nanotechnology* **2013**, *24*, 465304.
[20] A. A. Kazemzadeh Farizhandi, S. Z. Khalajabadi, V. Krishnadoss, I. Noshadi, *J. Mech. Behav. Biomed. Mater.* **2020**, *110*, 103960.
[21] R. Yang, X. Chen, Y. Zheng, K. Chen, W. Zeng, X. Wu, *J. Mater. Chem. C* **2022**, *10*, 5380.
[22] G. Liu, Y. Gao, S. Xu, T. Bu, Y. Xie, C. Xu, H. Zhou, Y. Qi, C. Zhang, *EcoMat* **2021**, *3*, e12130.
[23] S. Alom Ruiz, C. S. Chen, *Soft Matter* **2007**, *3*, 168.
[24] G. Liu, M. Rong, H. Hu, L. Chen, Z. Xie, Z. Zheng, *Adv. Mater. Technol.* **2022**, *7*, 2101493.
[25] G. Liu, S. H. Petrosko, Z. Zheng, C. A. Mirkin, *Chem. Rev.* **2020**, *120*, 6009.
[26] G. Liu, M. Hirtz, H. Fuchs, Z. Zheng, *Small* **2019**, *15*, 1900564.
[27] S. Khan, L. Lorenzelli, R. S. Dahiya, *IEEE Sens. J.* **2015**, *15*, 3164.
[28] D.-H. Kim, N. Lu, R. Ma, Y.-S. Kim, R.-H. Kim, S. Wang, J. Wu, S. M. Won, H. Tao, A. Islam, K. J. Yu, T.-I. Kim, R. Chowdhury, M. Ying, L. Xu, M. Li, H.-J. Chung, H. Keum, M. Mccormick, P. Liu, Y.-W. Zhang, F. G. Omenetto, Y. Huang, T. Coleman, J. A. Rogers, *Science* **2011**, *333*, 838.
[29] N. L. Rosi, C. A. Mirkin, *Chem. Rev.* **2005**, *105*, 1547.
[30] H. Hu, X. Guo, Y. Zhang, Z. Chen, L. Wang, Y. Gao, Z. Wang, Y. Zhang, W. Wang, M. Rong, G. Liu, Q. Huang, Y. Zhu, Z. Zheng, *ACS Nano* **2023**, *17*, 3921.
[31] P. Van Assenbergh, E. Meinders, J. Geraedts, D. Dodou, *Small* **2018**, *14*, 1703401.
[32] Z. J. Chen, X. Lu, H. X. Wang, J. Chang, D. R. Wang, W. S. Wang, S. W. Ng, M. M. Rong, P. Li, Q. Y. Huang, Z. F. Gan, J. W. Zhong, W. D. Li, Z. J. Zheng, *Adv. Mater.* **2023**, *35*, 2101493.
[33] M. Huff, *Micromachines* **2021**, *12*, 991.
[34] E. Albert, N. Cotolan, N. Nagy, G. Sáfrán, G. Szabó, L.-M. Muresan, Z. Hórvölgyi, *Microporous Mesoporous Mater.* **2015**, *206*, 102.
[35] Y. Zhang, X. Guo, J. Huang, Z. Ren, H. Hu, P. Li, X. Lu, Z. Wu, T. Xiao, Y. Zhu, G. Li, Z. Zheng, *npj Flexible Electron.* **2022**, *6*, 4.
[36] J. X. Cai, C. P. Zhang, A. Khan, L. Q. Wang, W. D. Li, *ACS Appl. Mater. Interfaces* **2018**, *10*, 28754.
[37] X. Lu, Y. Zhang, Z. Zheng, *Adv. Electron. Mater.* **2021**, *7*, 2001121.

[38] A. Khan, C. Liang, Y.-T. Huang, C. Zhang, J. Cai, S.-P. Feng, W.-D. Li, *Adv. Eng. Mater.* **2019**, *21*, 1900723.
[39] G. Haacke, *J. Appl. Phys.* **1976**, *47*, 4086.
[40] J. Schneider, P. Rohner, D. Thureja, M. Schmid, P. Galliker, D. Poulikakos, *Adv. Funct. Mater.* **2016**, *26*, 833.
[41] D.-S. Leem, A. Edwards, M. Faist, J. Nelson, D. D. C. Bradley, J. C. De Mello, *Adv. Mater.* **2011**, *23*, 4371.
[42] H.-Z. Geng, K. K. Kim, K. P. So, Y. S. Lee, Y. Chang, Y. H. Lee, *J. Am. Chem. Soc.* **2007**, *129*, 7758.
[43] S. Bae, H. Kim, Y. Lee, X. Xu, J.-S. Park, Y. Zheng, J. Balakrishnan, T. Lei, H. Ri Kim, Y. I. Song, Y.-J. Kim, K. S. Kim, B. Özyilmaz, J.-H. Ahn, B. H. Hong, S. Iijima, *Nat. Nanotechnol.* **2010**, *5*, 574.
[44] S. Lin, X. Bai, H. Wang, H. Wang, J. Song, K. Huang, C. Wang, N. Wang, B. Li, M. Lei, H. Wu, *Adv. Mater.* **2017**, *29*, 1703238.
[45] A. Khan, S. Lee, T. Jang, Z. Xiong, C. Zhang, J. Tang, L. J. Guo, W.-D. Li, *Small* **2016**, *12*, 3021.
[46] H. Wu, D. Kong, Z. Ruan, P.-C. Hsu, S. Wang, Z. Yu, T. J. Carney, L. Hu, S. Fan, Y. Cui, *Nat. Nanotechnol.* **2013**, *8*, 421.
[47] B. Han, K. Pei, Y. Huang, X. Zhang, Q. Rong, Q. Lin, Y. Guo, T. Sun, C. Guo, D. Carnahan, M. Giersig, Y. Wang, J. Gao, Z. Ren, K. Kempa, *Adv. Mater.* **2014**, *26*, 873.
[48] H.-J. Kim, S.-H. Lee, J. Lee, E.-S. Lee, J.-H. Choi, J.-H. Jung, J.-Y. Jung, D.-G. Choi, *Small* **2014**, *10*, 3767.
[49] S. Kiruthika, R. Gupta, K. D. M. Rao, S. Chakraborty, N. Padmavathy, G. U. Kulkarni, *J. Mater. Chem. C* **2014**, *2*, 2089.
[50] S. Hong, J. Yeo, G. Kim, D. Kim, H. Lee, J. Kwon, H. Lee, P. Lee, S. H. Ko, *ACS Nano* **2013**, *7*, 5024.
[51] H.-J. Choi, S. Choo, P.-H. Jung, J.-H. Shin, Y.-D. Kim, H. Lee, *Nanotechnology* **2015**, *26*, 055305.
[52] Z. Zhao, Q. Huang, C. Yan, Y. Liu, X. Zeng, X. Wei, Y. Hu, Z. Zheng, *Nano Energy* **2020**, *70*, 104528.
[53] X. Tao, S. Liao, Y. Wang, *EcoMat* **2021**, *3*, e12083.
[54] Z. Liu, K. Chen, A. Fernando, Y. Gao, G. Li, L. Jin, H. Zhai, Y. Yi, L. Xu, Y. Zheng, H. Li, Y. Fan, Y. Li, Z. Zheng, *Chem. Eng. J.* **2021**, *403*, 126191.
[55] J. Xue, Y. Zou, Y. Deng, Z. Li, *EcoMat* **2022**, *4*, e12209.
[56] J. Y. Wang, N. N. Yang, G. Cheng, J. Y. Ji, *J. Mater. Sci.: Mater. Electron.* **2023**, *34*, 930.
[57] T. Farid, M. I. Rafiq, A. Ali, W. Tang, *EcoMat* **2022**, *4*, e12154.
[58] Y. Joo, J. Byun, N. Seong, J. Ha, H. Kim, S. Kim, T. Kim, H. Im, D. Kim, Y. Hong, *Nanoscale* **2015**, *7*, 6208.
[59] J. Luo, Z. L. Wang, *EcoMat* **2020**, *2*, e12059.